Steady-State Analysis of Inductor Conduction Modes in the Quadratic Boost Converter

Oswaldo Lopez-Santos*, *Student Member, IEEE,* Luis Martinez-Salamero, *Senior Member, IEEE*, Germain Garcia, Hugo Valderrama-Blavi, *Member, IEEE,* and David Zambrano-Prada

Abstract

The conduction modes of the quadratic boost converter are explored in the context of high DC gain applications. A complete analytical description of the steady-state behavior of the converter operating in four possible inductor current discontinuous conduction modes is presented. Boundaries between modes are determined together with the corresponding transitions. The study covers the operation of the converter using a pulse width modulator (PWM) for constant switching frequency, and employing a hysteresis comparator for variable switching frequency. Both cases are analyzed for the same set of converter parameters and different constant resistive loads, while the converter is fed by a low DC voltage ranging from 20 to 30 VDC. Several simulations are used to verify both waveforms and average values of the theoretical predictions. Experimental results in a 60 W prototype are in good agreement with the theoretical predictions, and efficiency measurements reveal that one of the discontinuous conduction modes can compete with the continuous conduction mode in high DC gain applications.

Index Terms

Quadratic boost converter, discontinuous conduction mode, high DC-gain converter.

I. INTRODUCTION

The interest for discontinuous conduction mode operation (DCM) in DC-DC converters goes back in time to the early years of modern power electronics in the beginning of 1970's. Although the development of computer programs for simulating DC-DC switching converters prompted many researchers to study DCM operation in a unified way [1]-[5], the industrial applications of DCM in all these years have been relatively marginal in comparison with the dominant operation in continuous conduction mode (CCM). Although quantitatively minor in applications, DCM is qualitatively preponderant in several important fields. Thus, it plays a significant role in the development of Power Factor Correction (PFC) rectifiers [6]-[10], and its use has been extended more recently to applications with microinverters [11]-[12], fuel- cells and battery storage [13]-[14], and also to electric vehicles [15]-[16]. A consequence of this revival has been a renovated interest for understanding both steady- state and dynamics of converters operating in discontinuous conduction mode, this originating additional generalized works [17]-[20]. Moreover, the development of advanced digital devices in the last decade has stimulated both discrete -time modeling [21]-[22] and digital implementation of converters operating in DCM [23]-[27]. All these works besides having allowed a better understanding of DC-DC converter features in DCM, they have also contributed to improve the converter performances in this conduction mode. It is recognized a reduction of size in components, a decrease of the switching losses and an increment in the speed of response. These advantages counterbalance in a great extent the drawbacks associated with higher current ripples and conduction losses.

The analysis of the discontinuous conduction mode in converters using Pulse Width Modulation (PWM) ,i.e. operating with constant switching frequency , has been solved for the second order converters buck, boost and buck-boost [28]-[32], and also for four order converters such Cûk and SEPIC [33]-[34]. More complex topologies of isolated [35]-[36] and interleaved converters [37]-[39] have been also studied in DCM operation. It is worth noting that the increase in the order of the converter can lead in DCM to a sequence of topological structures, which can be only disclosed after a dedicated analysis rather than after a more general approach [40].

The properties of DC-DC switching converters are interesting not only in CCM or DCM but also in the boundary between these two modes. In fact, a way to preserve the advantages of both modes consists in working in the Boundary Conduction Mode (BCM) [41]-[43]. However, this implies an additional study in terms of modelling and supplementary control functions detecting that mode [44].

As it is shown in [45], the boost converter in DCM exhibits a higher DC-gain with lower values of the duty cycle. Searching similar phenomena in other boost- derived converter topologies (i.e. quadratic boost, cubic boost and n-th boost converters [46]- [47]) can be useful for engineers in view of some recent developments of power distributed systems with high DC voltage levels (380 - 400 VDC) [48]-[49].

The quadratic boost converter stirs up a special interest because it combines a transformer-less topology of only one-controlled switch with a very high DC gain. Further, as shown in [50]-[51], this feature is especially attractive when the converter in CCM is controlled through a hysteresis modulator due to the possibility of working with very high values of the duty cycle avoiding modulator saturation.

The main goal of this paper is to explore the behavior of the quadratic boost in DCM high-gain operation by studying all possible modes and the transitions among them in order to eventually assess its potential applications. Thus, the steady -state analysis for constant switching frequency reveals the existence of three different DCM modes with higher DC-gain than that of CCM. The analysis for variable switching frequency reveals that only one of the previous modes can be attained when a hysteresis modulator is employed.

The rest of the paper is organized as follows: the study of circuit configurations and a general description of the converter are shown in section II. The expressions relating the converter variables, static gain function and boundary conditions for constant switching frequency operation are derived in chapter III. The study of DCM when the converter operates with variable switching frequency is presented in chapter IV. The theoretical predictions for both constant and variable switching frequency operation are verified by means of simulation in chapter V and by experimental results in chapter VI. Finally, conclusions of the work are given in chapter VII.

II. CIRCUIT CONFIGURATIONS AND DISCONTINUOUS CONDUCTION MODES

As it is shown in figure 1, the quadratic boost converter has five possible structures, namely those of figures 1a and 1b corresponding to a continuous conduction mode, and three additional topologies which, in conjugation with the first two ones, describe respectively three possible discontinuous conduction modes. Two of these structures are attained when only one inductor current, either L_1 or L_2 , reaches zero before a switching period is finished, thus originating the DCL1 state shown in figure 1c (Discontinuous Conduction on inductor L_1) or the DCL2 state shown in figure 1d (Discontinuous Conduction on inductor L_2)

respectively. The last structure shown in figure 1e is found when the current of both inductors reaches the zero value before a switching period is finished (DCL12 state).

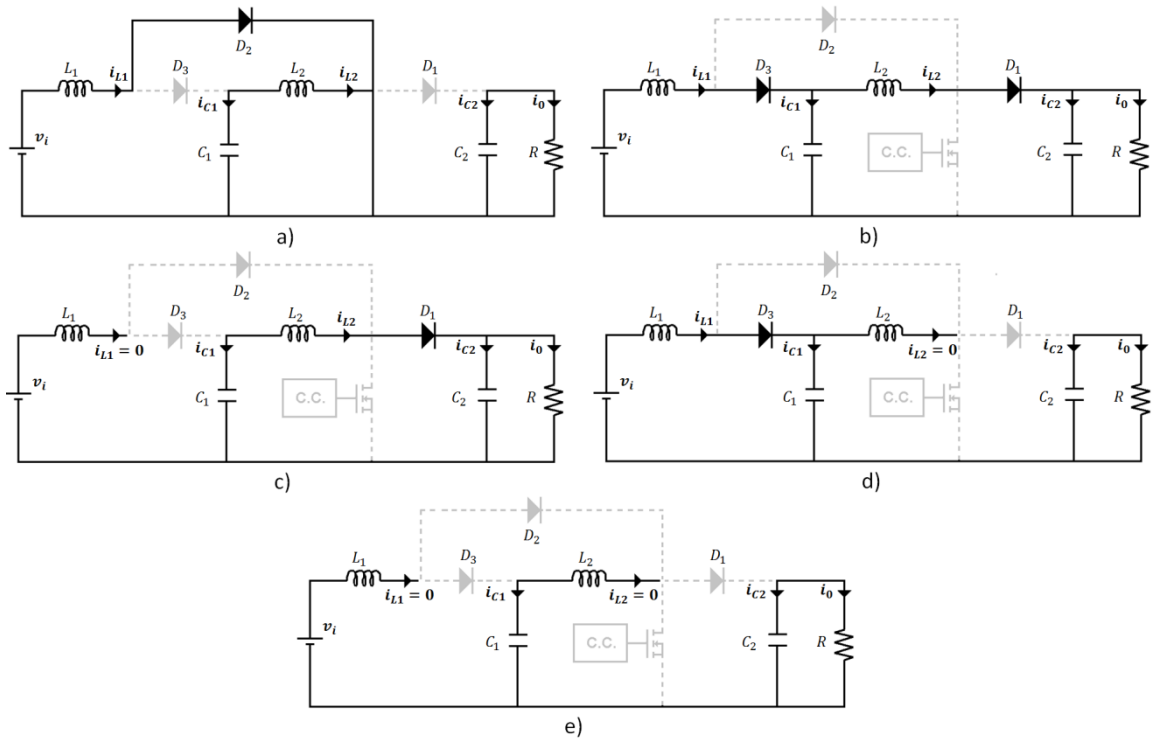

Fig.1. Circuit configurations of quadratic boost converter: a) on-state; b) off-state: c) DCL1-state; d) DCL2-state; and, e) DCL12-state.

From the above description, the quadratic boost converter can be modeled as a variable structure system which commutes between two, three or four structures during a switching period ($T_s = 1/f_s$) originating one of its different conduction modes. The five possible conduction modes are depicted in figure 2. As shown in figure 2b, if the structure of the system changes from the off-state to the on-state at the start of the switching period and from the on-state to the off-state when the interval defined by the duty cycle of the control signal is finished, then the converter operates in CCM. On the other hand, in the conduction modes DCL1 and DCL2, shown in figures 2c and 2d respectively, the converter changes from the off-state to either DCL1-state or DCL2-state and after that returns to the on-state at the beginning of a new switching period. Additionally, as shown in figures 2e and 2f, the converter can operate in either mode DCL12, i.e. arriving to DCL12-state from DCL1-state, or in the mode DCL21 arriving to DCL12-state from DCL2-state. The difference between these two last modes is the state that is firstly attained after the off-state.

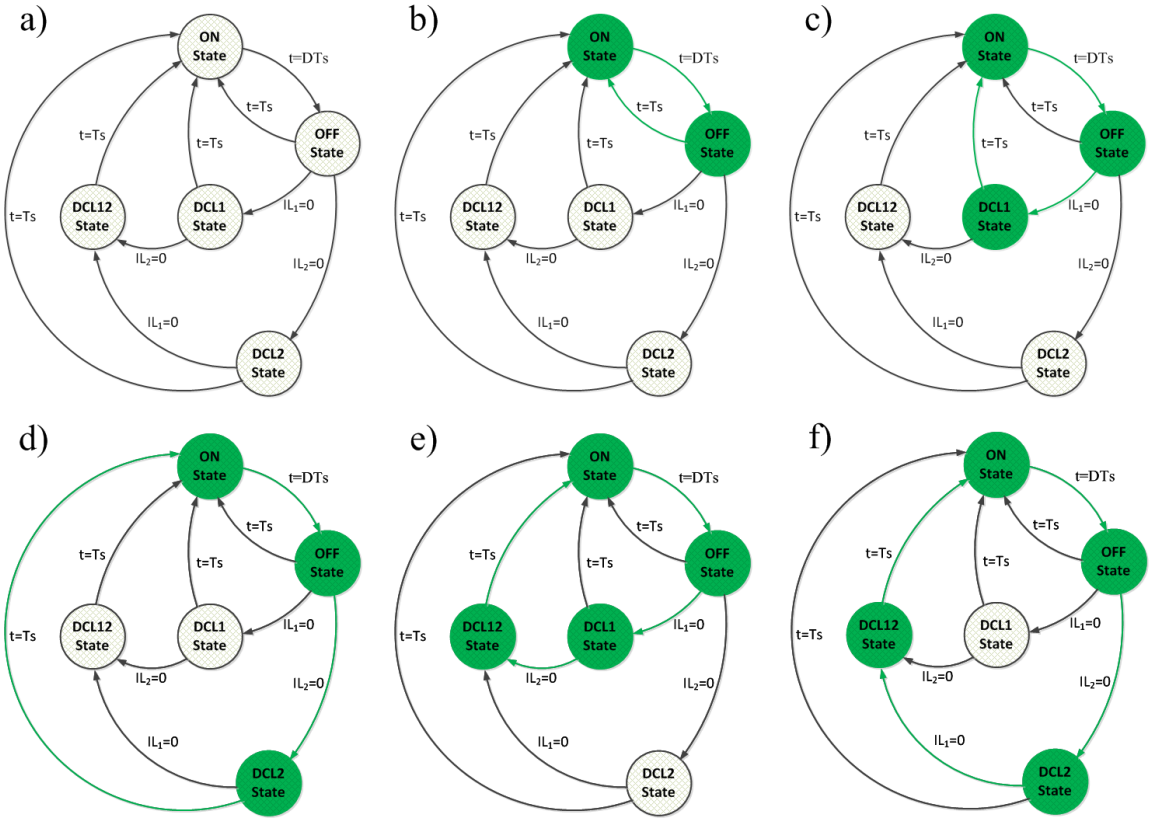

Fig. 2. Event diagram of the quadratic boost converter conduction modes: a) general representations of states and transitions, b) CCM mode, c) DCL1 mode, d) DCL2 mode, e) DCL12 mode, f) DCL21 mode.

For a given set of parameters of a converter with a PWM- based control system, the five modes can be always attained depending in each case on input and output conditions. However, if a hysteresis- based controller is used, then not all of the states will be reachable. Figure 3 shows the possible states and transitions for a quadratic boost converter controlled from the input inductor current using a hysteresis- based modulator with a current reference I_{ref} and a hysteresis band of 2Δ.

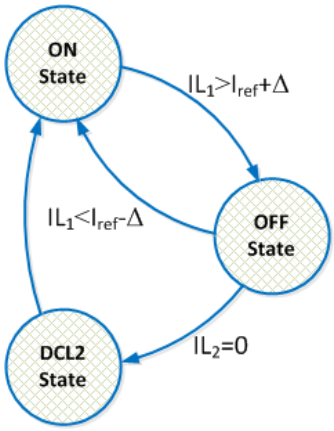

Fig. 3. Event diagram of the quadratic boost converter using a hysteresis comparator.

In this case, if the converter is in on-state, the change to off-state will depend on the instantaneous value of the input inductor current. In off-state, the converter can change to either on-state or DCL2-state. In turn, in DCL2-state, the converter can only change to on-state provided the input inductor is externally forced to remain in continuous conduction mode. However, to operate in this way and preserve the continuous conduction on the input inductor current, it is required that $I_{ref} > \Delta$ and also that Δ be sufficiently small.

From the above description, four different conduction modes are defined: CCM, DCL1, DCL2 and DCL12. Their dynamic behavior is defined by the corresponding set of differential equations summarized in Table I, which is associated to each circuit diagram in figure 2.

TABLE I
Set of differential equations of the converter states

	ON-State	**OFF-State**	**DCL1-State**	**DCL2-State**	**DCL12-State**
$v_{L1} = L_1 \frac{di_{L1}}{dt}$	v_{in}	$v_{in} - v_{C1}$	0	$v_{in} - v_{C1}$	0
$v_{L2} = L_2 \frac{di_{L2}}{dt}$	v_{C1}	$v_{C1} - v_{C2}$	$v_{C1} - v_{C2}$	0	*0*
$i_{C1} = C_1 \frac{dv_{C1}}{dt}$	$-i_{L2}$	$i_{L1} - i_{L2}$	$-i_{L2}$	i_{L1}	*0*
$i_{C2} = C_2 \frac{dv_{C2}}{dt}$	$-\frac{v_{C2}}{R}$	$i_{L2} - \frac{v_{C2}}{R}$	$i_{L2} - \frac{v_{C2}}{R}$	$-\frac{v_{C2}}{R}$	$-\frac{v_{C2}}{R}$

From the equations in Table I, a compact representation can be obtained using the following multi-linear expression

$$\begin{aligned}
\frac{di_{L1}}{dt} &= \frac{v_{in}}{L_1}(1-u_1) - \frac{v_{C1}}{L_1}(1-u-u_1) \\
\frac{di_{L2}}{dt} &= \frac{v_{C1}}{L_2}(1-u_2) - \frac{v_{C2}}{L_2}(1-u-u_2) \\
\frac{dv_{C1}}{dt} &= -\frac{i_{L2}}{C_1}(1-u_2) + \frac{i_{L1}}{C_1}(1-u-u_2) \\
\frac{dv_{C2}}{dt} &= \frac{i_{L2}}{C_2}(1-u-u_2) - \frac{v_{C2}}{RC_2}
\end{aligned} \tag{1}$$

where u is the control signal of the controlled switch, and u_1 and u_2 model respectively the existence of DCL1 and DCL2. Variable u_1 takes the value 1 when the converter operates in DCL1, and the variable u_2 takes the value 1 when the converter operates in the mode DCL2. In mode DCL12, both u_1 and u_2 take the value 1.Otherwise, both u_1 and u_2 take the value 0.

III. STEADY-STATE OF THE CONVERTER FOR CONSTANT SWITCHING FREQUENCY

From (1), it can be deduced the static gain of the converter as a function of either duty cycle (CCM) or duty cycle and output load (DCL1, DCL2 and DCL12 modes). It is also possible to obtain the static relations between the average values of either capacitor voltages and input voltage or inductor currents and load current. The mean values of the converter variables in steady-state will be represented by the notation $\langle\cdot\rangle$, while the control signal u will be substituted by its average value U.

A. Converter operating in CCM

From the expressions listed in Table I, the energy balance in a switching period in inductors and capacitors in steady-state is the following

$$\langle v_{L1}\rangle = \frac{\langle v_{in}\rangle UT_s + (\langle v_{in}\rangle - \langle v_{C1}\rangle)(1-U)T_s}{T_s} = 0 \tag{2}$$

$$\langle v_{L2}\rangle = \frac{\langle v_{C1}\rangle UT_s + (\langle v_{C1}\rangle - \langle v_{C2}\rangle)(1-U)T_s}{T_s} = 0 \tag{3}$$

$$\langle i_{C1}\rangle = \frac{-\langle i_{L2}\rangle UT_s + (-\langle i_{L2}\rangle + \langle i_{L1}\rangle)(1-U)T_s}{T_s} = 0 \tag{4}$$

$$\langle i_{C2}\rangle = \frac{-\frac{\langle v_{C2}\rangle}{R}UT_s + \left(\langle i_{L2}\rangle - \frac{\langle v_{C2}\rangle}{R}\right)(1-U)T_s}{T_s} = 0 \tag{5}$$

Denoting $V_{in} = \langle v_{in}\rangle$, the mean values of the converter variables are given by

$$\langle i_{L1}\rangle = I_{L1} = \frac{V_{in}}{R(1-U)^4} \tag{6}$$

$$\langle i_{L2}\rangle = I_{L2} = \frac{V_{in}}{R(1-U)^3} \tag{7}$$

$$\langle v_{C1}\rangle = V_{C1} = \frac{V_{in}}{(1-U)} \tag{8}$$

$$\langle v_{C2}\rangle = V_{C2} = \frac{V_{in}}{(1-U)^2} \tag{9}$$

Hence, the ideal static gain of the converter will be expressed as

$$M_{CCM}(U) = \frac{V_{C2}}{V_{in}} = \frac{1}{(1-U)^2} \tag{10}$$

B. Converter operating in DCL1 mode

Similarly, energy balance in L_1, L_2 and C_2 implies

$$\langle v_{L1} \rangle = \frac{\langle v_{in} \rangle U T_s + (\langle v_{in} \rangle - \langle v_{C1} \rangle) U_1 T_s}{T_s} = 0 \tag{11}$$

$$\langle v_{L2} \rangle = \frac{\langle v_{C1} \rangle U T_s + (\langle v_{C1} \rangle - \langle v_{C2} \rangle)(1-U) T_s}{T_s} = 0 \tag{12}$$

$$\langle i_{C2} \rangle = \frac{-\frac{\langle v_{C2} \rangle}{R} U T_s + \left(\langle i_{L2} \rangle - \frac{\langle v_{C2} \rangle}{R} \right)(1-U) T_s}{T_s} = 0 \tag{13}$$

By solving (11), (12) and (13), the steady-state expressions for v_{C1}, v_{C2} and i_{L2} are obtained.

$$\langle v_{C1} \rangle = V_{C1} = \frac{\langle v_{in} \rangle (U + U_1)}{U_1} \tag{14}$$

$$\langle v_{C2} \rangle = V_{C2} = \frac{\langle v_{in} \rangle (U + U_1)}{U_1 (1-U)} \tag{15}$$

$$\langle i_{L2} \rangle = I_{L2} = \frac{\langle v_{C2} \rangle}{R(1-U)} \tag{16}$$

The average value of i_{L1} can be obtained from the current waveform shown in figure 4. The height of the triangle is defined by the maximum value of i_{L1}, which is denoted as I_{L1max} whereas the base is defined by the time interval $(U + U_1)T_s$.

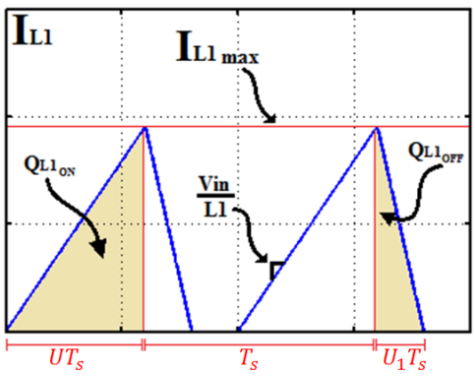

Fig. 4. Current waveform of the inductor L1 when the converter operates in DCL1 mode.

The value of $I_{L1_{max}}$ can be obtained using the slope of the inductor current in the on-state as follows

$$I_{L1_{max}} = \left(\frac{\langle v_{in}\rangle}{L_1}\right) UT_s \tag{17}$$

Then, we have

$$\langle i_{L1}\rangle = \frac{\langle v_{in}\rangle U(U+U_1)}{2L_1 f_s} \tag{18}$$

Therefore, the charge balance in C_1 leads to

$$\langle i_{C1}\rangle = \frac{-\langle i_{L2}\rangle T_s + Q_{L1_{OFF}}}{T_s} = 0 \tag{19}$$

where $Q_{L1_{OFF}}$ represents the charge given by inductor L_1 to capacitor C_1 across diode D_3. Its value can be determined as the area below the current waveform in figure 5.

$$Q_{L1_{OFF}} = \frac{\langle v_{in}\rangle U U_1 T_s}{2L_1 f_s} = \frac{U_1 T_s}{2} I_{L1_{max}} \tag{20}$$

Thus, by replacing (20) in (19), another steady-state expression for i_{L2} is obtained.

$$\langle i_{L2}\rangle = \frac{\langle v_{in}\rangle U U_1}{2L_1 f_s} \tag{21}$$

By equaling expressions (16) and (21), it is possible to obtain K_1, which is a standard parameter to analyze the discontinuous conduction mode [45].

$$K_1 = \frac{2L_1}{RT_s} = \frac{U(1-U)^2 {U_1}^2}{U+U_1} \tag{22}$$

After that, extracting $\langle v_{in}\rangle/\langle v_{C2}\rangle$ from (15) and replacing in (22), the value of U_1 is given by

$$U_1 = K_1\left(\frac{\langle v_{C2}\rangle}{\langle v_{in}\rangle}\right)\left(\frac{1}{U(1-U)}\right) = \frac{K_1}{2U(1-U)^2}\left(1+\sqrt{1+\frac{4U^2(1-U)^2}{K_1}}\right) \quad (23)$$

From the aforementioned expressions, the mean values of the converter variables are given by

$$\langle i_{L1}\rangle = I_{L1} = \frac{V_{in}}{4R(1-U)^2}\left(1+\sqrt{1+\frac{4U^2(1-U)^2}{K_1}}\right)^2 \quad (24)$$

$$\langle i_{L2}\rangle = I_{L2} = \frac{V_{in}}{2R(1-U)^2}\left(1+\sqrt{1+\frac{4U^2(1-U)^2}{K_1}}\right) \quad (25)$$

$$\langle v_{C1}\rangle = V_{C1} = \frac{V_{in}}{2}\left(1+\sqrt{1+\frac{4U^2(1-U)^2}{K_1}}\right) \quad (26)$$

$$\langle v_{C2}\rangle = V_{C2} = \frac{V_{in}}{2(1-U)}\left(1+\sqrt{1+\frac{4U^2(1-U)^2}{K_1}}\right) \quad (27)$$

Finally, the voltage conversion ratio of the converter operating in DCL1 can be expressed

$$M_{DCM1}(U) = \frac{V_{C2}}{V_{in}} = \frac{1+\sqrt{1+\frac{4U^2(1-U)^2}{K_1}}}{2(1-U)} \quad (28)$$

C. Converter operating in DCL2 mode

From the expressions listed in table I, the volts-second balances are given by

$$\langle v_{L1}\rangle = \frac{\langle v_{in}\rangle UT_s + (\langle v_{in}\rangle - \langle v_{C1}\rangle)(1-U)T_s}{T_s} = 0 \quad (29)$$

$$\langle v_{L2}\rangle = \frac{\langle v_{C1}\rangle UT_s + (\langle v_{C1}\rangle - \langle v_{C2}\rangle)U_2T_s}{T_s} = 0 \quad (30)$$

By solving (29) and (30), the steady-state expressions for v_{C1} and v_{C2} are obtained

$$\langle v_{C1}\rangle = \frac{\langle v_{in}\rangle}{1-U} \tag{31}$$

$$\langle v_{C2}\rangle = \frac{\langle v_{in}\rangle(U+U_2)}{U_2(1-U)} \tag{32}$$

There are two charges involved in the charge balance of capacitor C_1. A positive charge is given by inductor L_1 during the interval $(1-U)T_s$ whereas a negative charge Q_{L2} is extracted for inductor L_2 during the interval $(U+U_2)T_s$. Then, we have

$$\langle i_{C1}\rangle = \frac{\langle i_{L1}\rangle(1-U)T_s - Q_{L2}}{T_s} = 0 \tag{33}$$

The value of Q_{L2} is obtained computing the area below the current waveform in figure 5 during the interval $(U+U_2)T_s$. The value of charge Q_{L2} divided by the switching period is the same mean value of inductor current i_{L2}. Hence, the following relation is obtained

$$\langle i_{L1}\rangle = \langle i_{L2}\rangle \frac{1}{(1-U)} \tag{34}$$

The value of Q_{L2} is obtained as the area of the triangle below the current waveform of inductor L_2 shown in figure 5b. The height of the triangle is defined by the maximum value of i_{L2}, denoted as I_{L2max}, whereas the basis is the interval $(U+U_2)T_s$. The value of I_{L2max} is derived using the slope of the inductor current in the on state

$$I_{L2max} = \left(\frac{\langle v_{C1}\rangle}{L_2}\right)UT_s = \frac{1}{L_2}\left(\frac{\langle v_{in}\rangle}{1-U}\right)UT_s \tag{35}$$

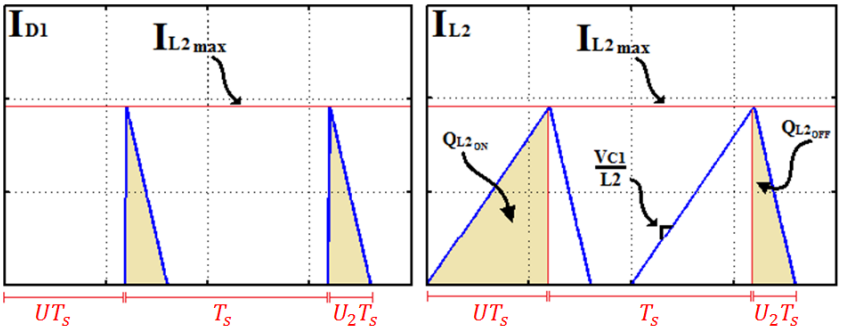

Fig. 5. Current waveforms when the converter operates in DCL2 mode: a) diode D1, b) inductor L2

and therefore , we obtain

$$Q_{L2} = \frac{\langle v_{in} \rangle}{2L_2 f_s} \frac{U(U+U_2)}{(1-U)} T_s \tag{36}$$

On the other hand, the charge balance in capacitor C_2 is solved considering the relation between the load current and the current of diode D_1 , which is shown in figure 3.6b. Hence, it is possible to derive equation (36) since the mean value of the output current is the same mean value of the current through diode D_1 (Q_{L2OFF}/T_s).

$$\frac{\langle v_{C2} \rangle}{R} = \langle i_{D1} \rangle = \frac{\langle v_{in} \rangle (U+U_2)}{RU_2(1-U)} \tag{37}$$

The mean value of the diode current is given by

$$\langle i_{D1} \rangle = \frac{1}{T_s}\left(\frac{1}{2} I_{L2max} U_2 T_s\right) = \frac{\langle v_{in} \rangle U U_2}{2L_2 f_s (1-U)} \tag{38}$$

By equaling expressions (37) and (38), it is obtained

$$K_2 = \frac{2L_2}{RT_s} = \frac{U{U_2}^2}{(U+U_2)} \tag{39}$$

By solving (32) for $\langle v_{C2} \rangle / \langle v_{in} \rangle$ and replacing in (39), the value of U_2 is deduced

$$U_2 = K_2 \left(\frac{\langle v_{C2} \rangle}{\langle v_{in} \rangle}\right)\left(\frac{1-U}{U}\right) = \frac{K_2}{U}\left(1 + \sqrt{1 + \frac{4U^2}{K_2}}\right) \tag{40}$$

From the abovementioned expressions, the mean values of the converter variables are given by

$$\langle i_{L1} \rangle = I_{L1} = \frac{V_{in}}{4R(1-U)^2}\left(1 + \sqrt{1 + \frac{4U^2}{K_2}}\right)^2 \tag{41}$$

$$\langle i_{L2}\rangle = I_{L2} = \frac{V_{in}}{4R(1-U)}\left(1+\sqrt{1+\frac{4U^2}{K_2}}\right)^2 \tag{42}$$

$$\langle v_{C1}\rangle = V_{C1} = \frac{V_{in}}{(1-U)} \tag{43}$$

$$\langle v_{C2}\rangle = V_{C2} = \frac{V_{in}}{2(1-U)}\left(1+\sqrt{1+\frac{4U^2}{K_2}}\right) \tag{44}$$

The voltage conversion ratio of the converter operating in DCL2 is

$$M_{DCM2}(U) = \frac{V_{C2}}{V_{in}} = \frac{1+\sqrt{1+\frac{4U^2}{K_2}}}{2(1-U)} \tag{45}$$

D. Converter operating in DCL12, DCL21 modes

From the expressions listed in table I, the balances in L_1 and L_2 are given by

$$\langle v_{L1}\rangle = \frac{\langle v_{in}\rangle UT_s + (\langle v_{in}\rangle - \langle v_{C1}\rangle)U_1T_s}{T_s} = 0 \tag{46}$$

$$\langle v_{L2}\rangle = \frac{\langle v_{C1}\rangle UT_s + (\langle v_{C1}\rangle - \langle v_{C2}\rangle)U_2T_s}{T_s} = 0 \tag{47}$$

By solving (46) and (47), the steady-state expressions for v_{C1} and v_{C2} are obtained.

$$\langle v_{C1}\rangle = \frac{\langle v_{in}\rangle(U+U_1)}{U_1} \tag{48}$$

$$\langle v_{C2}\rangle = \frac{\langle v_{C1}\rangle(U+U_2)}{U_2} \tag{49}$$

The charge balances in both capacitors C_1 and C_2 can be obtained from the current waveforms shown in figure 6.

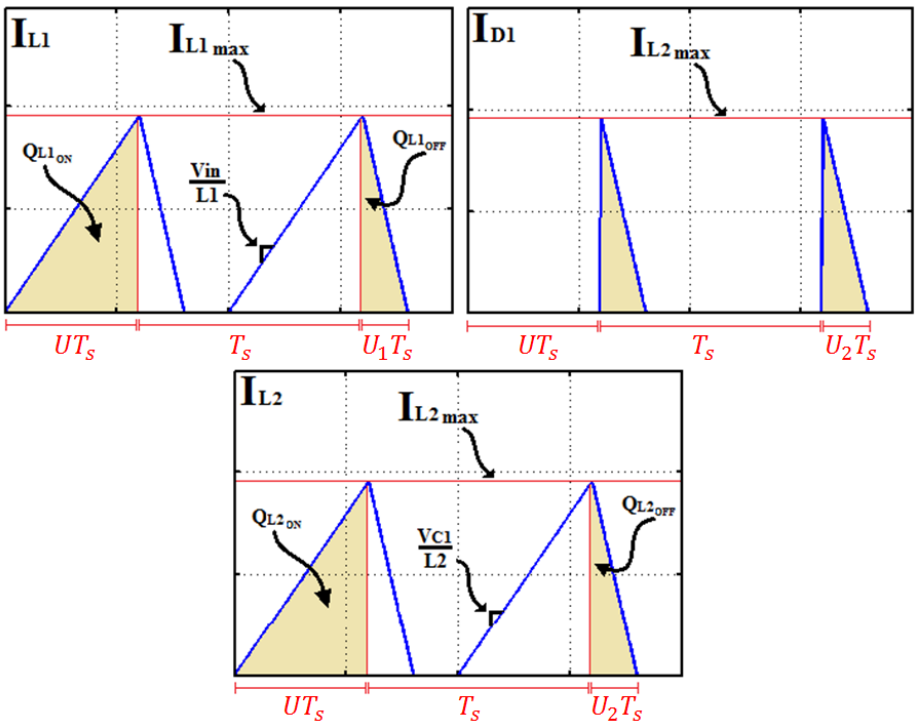

Fig. 6. Current waveforms when the converter operates in DCL12 : a) inductor L1, b) diode D1, c) inductor L2.

$$\langle i_{C1}\rangle = \frac{Q_{L1_{OFF}} - Q_{L2}}{T_s} = \frac{1}{T_s}\left(\frac{I_{L1_{max}} U_1 T_s}{2}\right) - \frac{1}{T_s}\left(\frac{I_{L2_{max}}(U+U_2)T_s}{2}\right) = 0 \tag{50}$$

$$\langle i_{C2}\rangle = \frac{Q_{L2_{OFF}}}{T_s} - \frac{\langle v_{C2}\rangle}{R} = \frac{1}{T_s}\left(\frac{I_{L2_{max}} U_2 T_s}{2}\right) - \frac{\langle v_{C2}\rangle}{R} = 0 \tag{51}$$

where the maximum values of the inductor currents are given by the expressions

$$I_{L1_{max}} = \left(\frac{\langle v_{in}\rangle}{L_1}\right) UT_s \tag{52}$$

$$I_{L2_{max}} = \left(\frac{\langle v_{C1}\rangle}{L_2}\right) UT_s \tag{53}$$

By replacing (52) and (53) in (50) and solving for the relation $\langle v_{C1}\rangle / \langle v_{in}\rangle$, we obtain

$$\frac{\langle v_{C1}\rangle}{\langle v_{in}\rangle} = \frac{L_2}{L_1}\left(\frac{U_1}{U+U_2}\right) \tag{54}$$

By defining constants K_1 and K_2 with the expressions

$$K_1 = \frac{2L_1}{RT_s} \tag{55}$$

$$K_2 = \frac{2L_2}{RT_s} \tag{56}$$

Then, from (54), (55) and (56), we have

$$\frac{\langle v_{C1}\rangle}{\langle v_{in}\rangle} = \frac{K_2}{K_1}\left(\frac{U_1}{U+U_2}\right) \tag{57}$$

Then, by replacing (56) in (51), we have

$$K_2 = \frac{U{U_2}^2}{U+U_2} = \frac{\langle v_{C1}\rangle}{\langle v_{C2}\rangle} U U_2 \tag{58}$$

By solving (58) for U_2 and replacing in (49), the following relation is obtained

$$M_a(U) = \frac{\langle v_{C2}\rangle}{\langle v_{C1}\rangle} = \frac{1+\sqrt{1+\frac{4U^2}{K_2}}}{2} \tag{59}$$

On the other hand, by replacing (58) in (57), it is derived that

$$\frac{\langle v_{C1}\rangle}{\langle v_i\rangle} = \left(\frac{1}{M_a(U)}\right)\frac{U_1 U U_2}{K_1(U+U_2)} \tag{60}$$

Then, solving (49) for $\langle v_{C1}\rangle/\langle v_{C2}\rangle$ and (48) for U_1, and replacing in (60), we deduce

$$\frac{\langle v_{C1}\rangle}{\langle v_{in}\rangle} = \frac{U^2}{K_1}\frac{\left(\frac{1}{M_a(U)}\right)^2}{\left(\frac{\langle v_{C1}\rangle}{\langle v_i\rangle}-1\right)}$$

Hence, the voltage conversion ratio of the converter operating in DCL12 can be expressed as

$$\frac{\langle v_{C2}\rangle}{\langle v_{in}\rangle}=\frac{V_{C2}}{V_{in}}=\frac{M_a(U)+\sqrt{[M_a(U)]^2+\frac{4U^2}{K_1}}}{2}=\frac{1}{2}\left(\left(\frac{\langle v_{C2}\rangle}{\langle v_{C1}\rangle}\right)+\sqrt{\left(\frac{\langle v_{C2}\rangle}{\langle v_{C1}\rangle}\right)^2+\frac{4U^2}{K_1}}\right)$$

$$M_{DCM12}(U)=\frac{V_{C2}}{V_{in}}=\frac{1}{4}\left(1+\sqrt{1+\frac{4U^2}{K_2}}+\sqrt{\left(1+\sqrt{1+\frac{4U^2}{K_2}}\right)^2+\frac{16U^2}{K_1}}\right) \quad (61)$$

From the aforementioned expressions, the mean values of the converter variables are given by

$$\langle v_{C1}\rangle = V_{C1} = V_{in}\frac{M_{DCM12}(U)}{M_a(U)} \quad (62)$$

$$\langle v_{C2}\rangle = V_{C2} = V_{in}[M_{DCM12}(U)] \quad (63)$$

From the input to output power balance, it is obtained that

$$\langle i_{L1}\rangle = I_{L1} = \frac{V_{in}[M_{DCM12}(U)]^2}{R} \quad (64)$$

Taking into account that $\langle i_{L2}\rangle = I_{L2_{max}}(U+U_2)/2$ and using (51) result in the following expression after some mathematical manipulation

$$\langle i_{L2}\rangle = I_{L2} = \frac{V_{in}M_{DCM12}(U)M_a(U)}{R} \quad (65)$$

E. Boundaries of the conduction modes

The boundaries between the different discontinuous conduction modes are obtained assuming that any inductor current reaches the zero value exactly at the end of the switching period. Then, it is possible to assert that the converter operates in a critical or boundary conduction mode. As expected, one or both parameters U_1 or U_2 are exactly equal to $1-U$, the use of this definition allowing the mathematical conditions derivation for the mode existence. The procedure consists in obtaining a critical value of K_1 or K_2 wherever it is possible to distinguish the operational modes. The values will be denoted $K_{1_{crit}}$ or $K_{2_{crit}}$ respectively. Four different boundaries can be identified:

a) The converter operates in CCM and the current of inductor L1 reaches the critical conduction mode, which is the way to enter in DCL1 mode.

By replacing $U_1 = 1 - U$ in (22), the following expression is obtained

$$K_{1_{crit}} = \frac{U(1-U)^2(1-U)^2}{U+(1-U)} = U(1-U)^4 \tag{66}$$

Then, it is possible to assert that when the converter operates in CCM the boundary to enter into DCL1 mode is defined by

$$\frac{2L_1}{RT_s} < U(1-U)^4 \tag{67}$$

b) The converter operates in CCM and the current of inductor L_2 reaches the critical conduction mode, which is the way to enter into DCL2 mode.

By replacing $U_2 = 1 - U$ in (38), it is obtained that

$$K_{2_{crit}} = \frac{U(1-U)^2}{U+(1-U)} = U(1-U)^2 \tag{68}$$

Then, it is possible to assert that when the converter operates in CCM, the boundary to attain DCL2 mode is defined by

$$\frac{2L_2}{RT_s} < U(1-U)^2 \tag{69}$$

c) The converter operates in DCL1 mode and the current of inductor L_2 reaches the critical conduction mode, which is the way to enter into DCL12 mode.

By replacing $U_2 = 1 - U$ in (58), the expression (68) is anew obtained. Then, it is possible to assert that, once in mode DCL1, the boundary to attain DCL12 mode is also defined by expression (69)

d) The converter operates in DCL2 mode and the current in inductor L_1 reaches the critical conduction mode, which is the way to enter into the DCL21 mode.

By replacing $U_1 = 1 - U$ in (48) and (57), and identifying the two expressions, we have

$$K_1 = K_2 \frac{(1-U)^2}{U + U_2} \tag{70}$$

On the other hand, by using relation (59), expression (58) becomes

$$K_2 = \frac{UU_2}{M_a(U)} \Rightarrow U_2 = \frac{M_a(U)K_2}{U} \tag{71}$$

Therefore (70) leads to

$$K_{1_{crit}} = \frac{2K_2U(1-U)^2}{2U^2 + K_2\left(1 + \sqrt{1 + \frac{4U^2}{K_2}}\right)} \tag{72}$$

Then, it is possible to conclude that when the converter operates in DCL2 mode, the boundary to attain DCL12 mode is defined by

$$\frac{2L_1}{RT_s} < \frac{2K_2U(1-U)^2}{2U^2 + K_2\left(1 + \sqrt{1 + \frac{4U^2}{K_2}}\right)} \tag{73}$$

Figure 7 shows the domains of the different conduction modes in terms of regions for CCM, DCL1, DCL2 and DCL12 as a function of the duty cycle U and DCM constants K_1 and K_2. As it can be observed, the discontinuous regions are concentrated around the low duty cycles and low values of K_1 and K_2, which correspond to low power levels. Note that the converter cannot work in the region of high duty cycles because the existence of the discontinuous conduction modes always requires the fulfilment of conditions $U_1 > 1 - U$ or $U_2 > 1 - U$ or both.

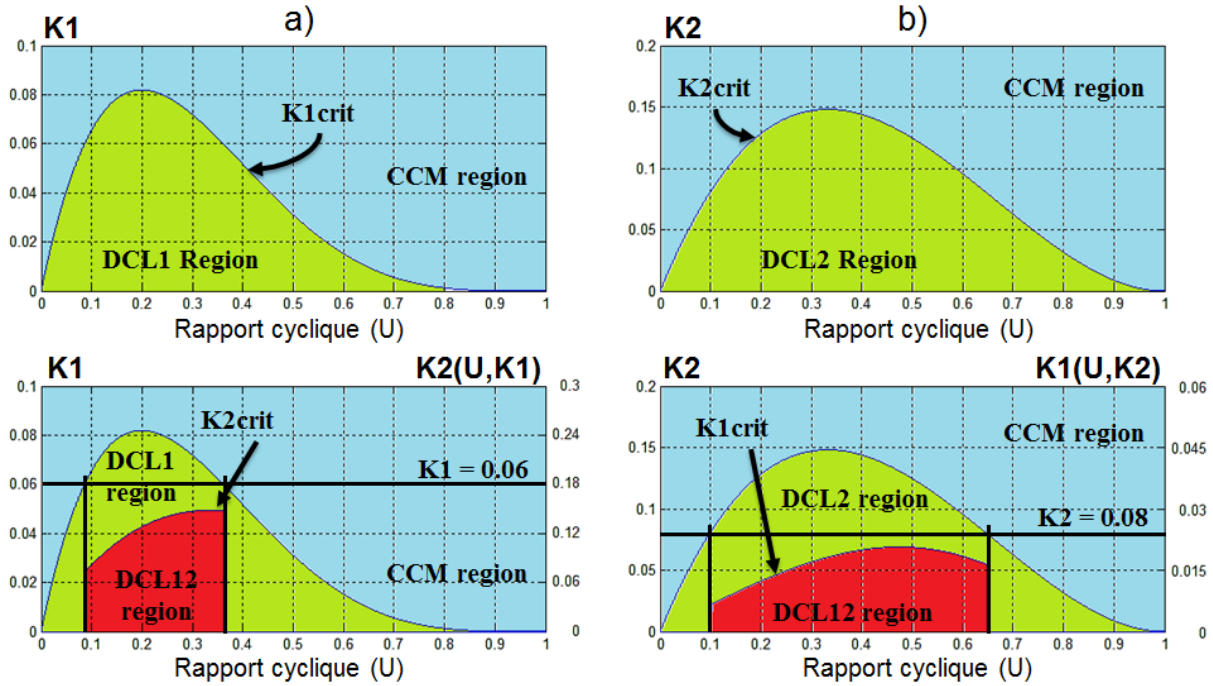

Fig.7. Graphical representation of critical values $K_{1_{crit}}$ and $K_{2_{crit}}$ as functions of duty cycle U: a) CCM and DCL1 (K_1 vs. U), b) CCM and DCL2 (K_2 vs. U), c) CCM, DCL1 and DCL12 (K_2 vs. U, K_1); d) CCM, DCL2 and DCL21 (K_1 vs. U, K_2).

As shown in figure 7, the critical values of K_1 and K_2 define the different limits between the conduction modes CCM, DCL1, DCL2 and DCL12. Figures 7a and 7b show the limits between CCM and modes DCL1 and DCL2 respectively. It is possible to observe that the region covered by mode DCL2 is considerably bigger than the region covered by mode DCL1. Besides, it is possible to observe in figures 7c and 7d that modes DCL12 and DCL21 can be only attained from DCL1 or DCL2 respectively for a delimited region of the duty cycle. This is due to the interdependence between the critical values $K_{1_{crit}}$ and $K_{2_{crit}}$ for the regions of DCL12 and DCL21 modes.

IV. STEADY-STATE OF THE CONVERTER FOR VARIABLE SWITCHING FREQUENCY

The use of a hysteresis comparator to implement a sliding-mode controller does not imply a change in the steady state behavior of the converter variables. However, it is necessary to consider that the different equilibrium points in the operational range of the converter have different switching frequencies. Then, first of all, it is necessary to consider that the system is limited to work in either CCM or DCL2 because the continuous conduction mode of inductor L1 ensures the sliding motion on the control surface [50]- [51]. However, it is possible to associate a duty cycle to each equilibrium point, and this fact is used to compare the two kinds of modulation employed in this work.

A. Operation in CCM

When operating in CCM with a hysteresis comparator, the converter has the same steady-state behavior than using a PWM modulator. This is mainly due to the fact that the gain and the steady state relations between variables are not dependent of the frequency. Therefore, expressions (6)-(9) remain valid.

B. Operation in DCL2 mode

When operating in DCL2, the steady- state gain of the converter and the relations among variables are a function of the resistive load and the switching frequency. Thus, from equations in the first row of Table I, it is obtained

$$t_{on} = \frac{2L_1\Delta}{V_{in}} = UT_s \tag{74}$$

$$t_{off} = \frac{2L_1\Delta}{V_{in} - V_{C1}} = (1-U)T_s \tag{75}$$

Then, the switching frequency is defined by

$$f_s = \frac{V_{in}U}{2L_1\Delta} \tag{76}$$

where Δ represents a hysteresis band.

Replacing (76) in (39), solving (8) for the duty cycle U and introducing the results in expression (74) yield

$$K_2 = \frac{2L_2 f_s}{R} = \frac{L_2 V_{in} U}{L_1 R \Delta} \tag{77}$$

Then, replacing (77) in expression (44), we obtain

$$V_{C2} = \frac{V_{in}}{2(1-U)}\left(1 + \sqrt{1 + \frac{4L_1 R\Delta U}{L_2 V_i}}\right) \tag{78}$$

C. *Boundary conduction mode between CCM and DCL2*

The boundary conduction mode between the two possible modes operating with variable switching frequency is determined by a value of the duty cycle defined as U_{crit} in expression (79), which is obtained by replacing (77) in (68).

$$U_{crit} = 1 - \sqrt{\frac{L_2 V_{in}}{L_1 R \Delta}} \tag{79}$$

V. SIMULATION RESULTS

A. *Converter gain and current waveforms for constant switching frequency*

Figure 10 depicts the gain of the converter for a set of converter parameters (L_1, L_2, C_1, C_2 and f_s) listed in the caption. The different conduction modes are represented as a function of the duty cycle and the output load *R*.

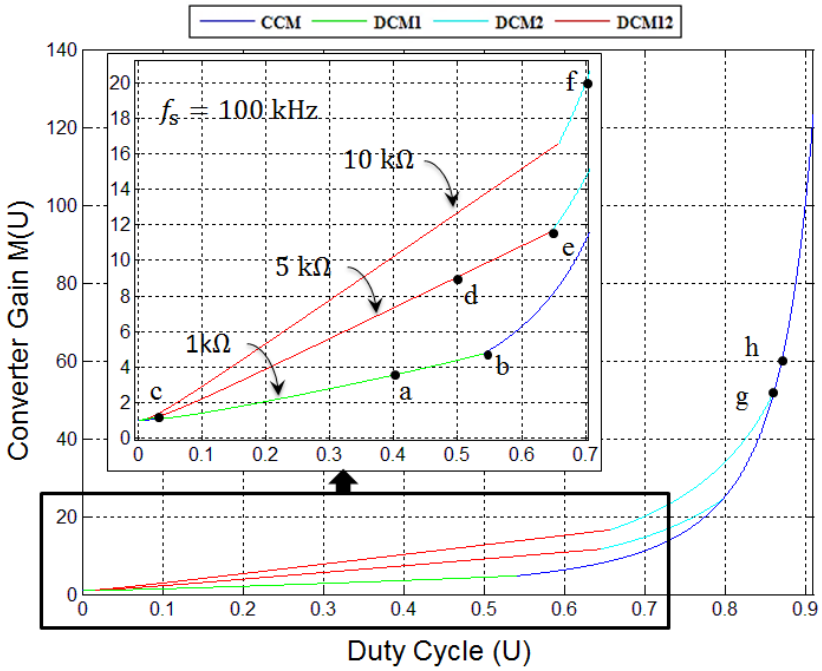

Fig.10. Ideal converter gain vs. duty cycle ($L_1 = 120\ \mu H, L_2 = 820\ \mu H, C_1 = C_2 = 10\ \mu F$)

Figure 10 also shows three curves of the converter gain *M(U)* as a function of the duty cycle *U*. Each one corresponds to a converter operation with a constant load resistance ($1k\Omega, 5k\Omega$ and $10k\Omega$). In these curves a distribution of the conduction modes can be observed. Different points (**a**, **b**, **c**, **d**, **e**, **f**, **g** and **h**) have been marked on the gain

characteristics to indicate a conduction mode or a limit between two of them. Further, each conduction mode has been highlighted by using the color code shown in the head of the figure. Point **a** ($U = 0.4$ and $M(U) = 3.546$) corresponds to DCL1 mode and point **b** ($U = 0.5411, M(U) = 4.748$) represents the boundary between DCL1 mode and CCM, both when the converter works with a load of 1 kΩ. Point **c** ($U = 0.0353, M(U) = 1.245$) is the boundary between DCL2 and DCL21, point **d** ($U = 0.5, M(U) = 9.057$) corresponds to DCL21 mode and point **e** ($U = 0.6464, M(U) = 11.61$) represents the boundary between DCL21 and DCL2. In the last three points the converter works with a load of 5 kΩ. Point **f** ($U = 0.7, M(U) = 19.96$) corresponds to DCL2, point **g** ($U = 0.8621, M(U) = 52.58$) belongs to the boundary between DCL2 mode and CCM, and point **h** ($U = 0.8709, M(U) = 60$) corresponds to CCM. For the last three points the converter works with a load of 10 kΩ. The validity of the predicted gains has been verified by means of PSIM simulations. The inductor current waveforms have been captured in each of the mentioned points in order to verify the corresponding conduction modes and boundaries. The results are shown in figure 11.

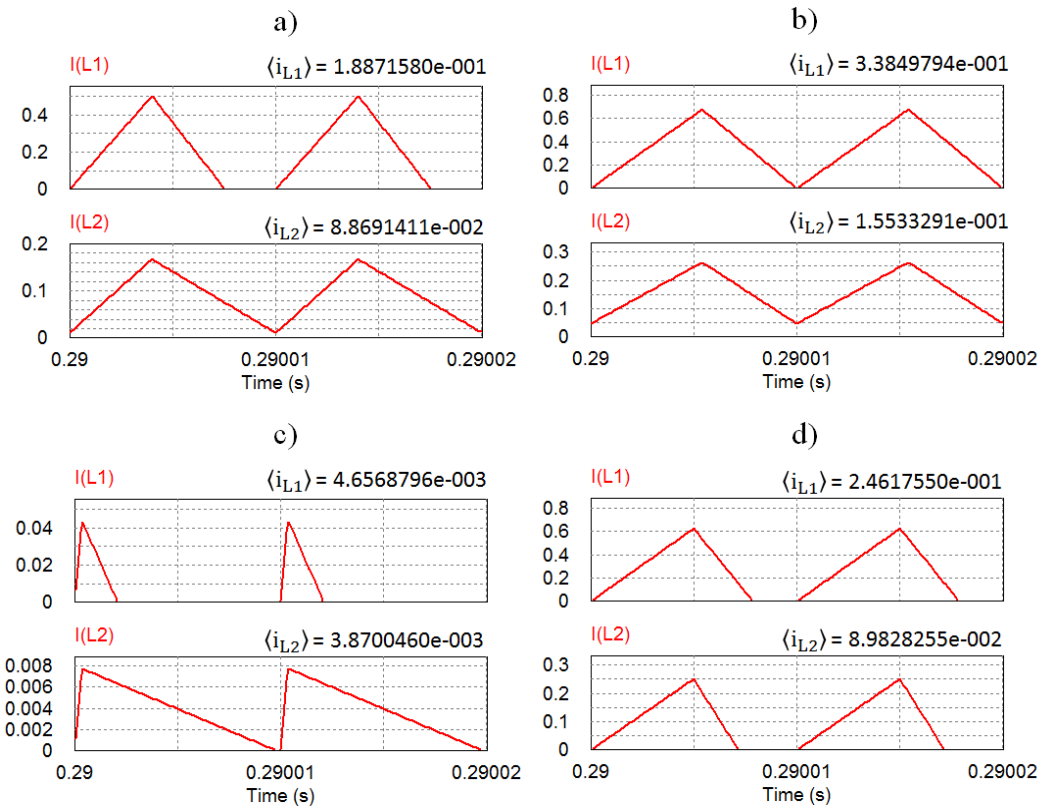

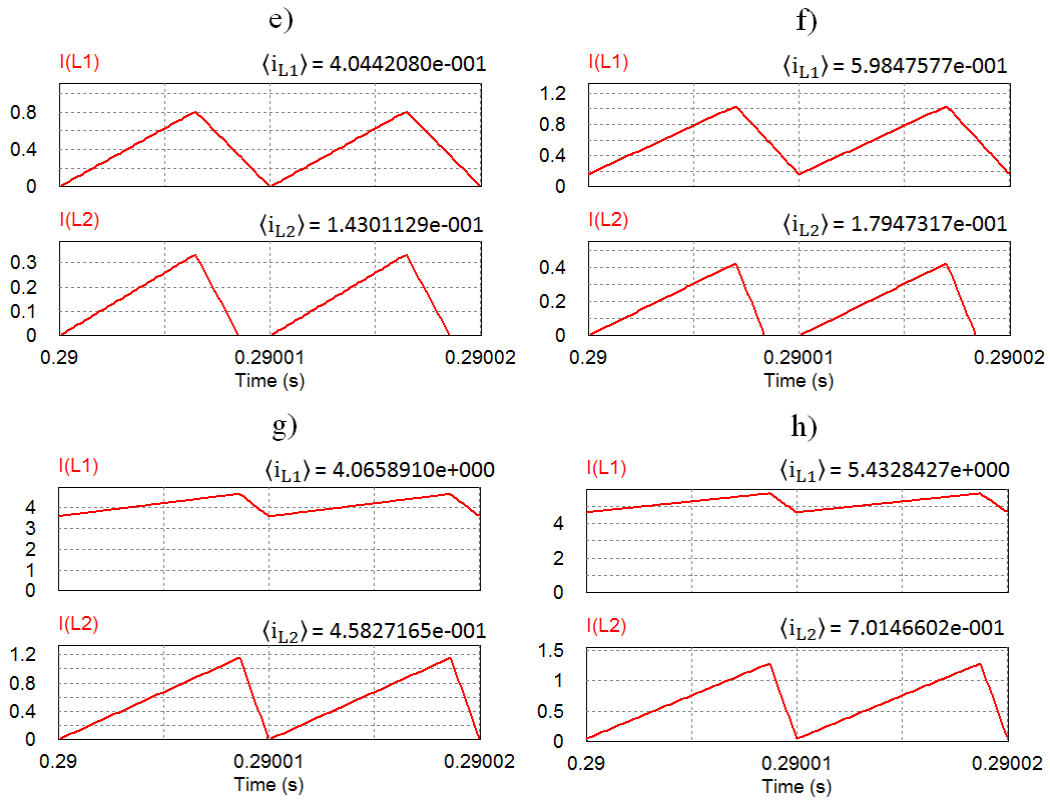

Fig.11. PSIM simulated waveforms of inductor currents for the operational points (a, b, c, d, e, f, g, h) in figure 10.

B. Converter gain for variable switching frequency

Figure 12 depicts the converter gain for the set of parameters (L_1, L_2, C_1, C_2) listed in the figure caption when the converter operates with variable switching frequency using a hysteresis comparator. The different conduction modes are represented as a function of the duty cycle and the output load *R*.

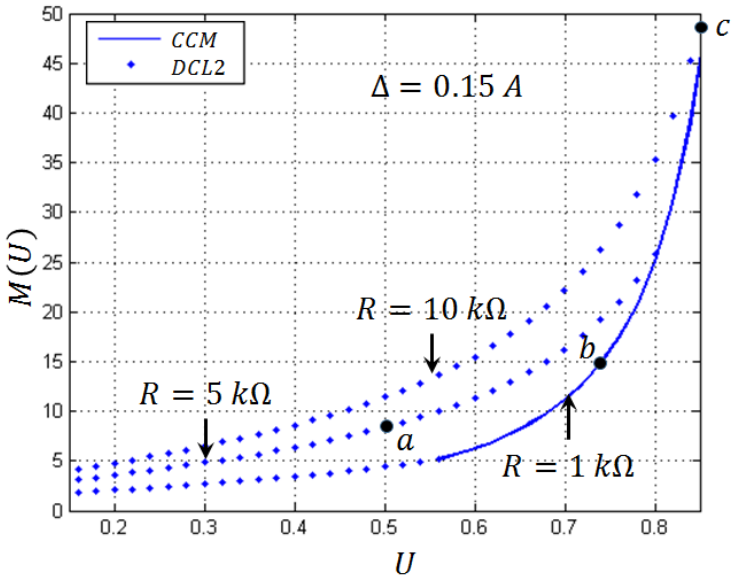

Fig.12. Ideal converter gain vs. duty cycle with variable frequency operation
(Parameters: $v_i = 15\,V, L_1 = 220\,\mu H, L_2 = 820\,\mu H, C_1 = C_2 = 10\,\mu F$)

Besides, three curves of the converter gain *M(U)* as a function of the duty cycle *U* are depicted. Each one corresponds to the converter operation with a constant load resistance ($1k\Omega, 5k\Omega$ and $10k\Omega$). Points **a**, **b**, and **c** have been marked on the gain characteristics to indicate the conduction modes CCM or DCL2, or a limit between them. Point **a** ($U = 0.5006, M(U) = 8.393$ and $f = 75\ kHz$) corresponds to DCL2 for a current reference of 0.59 A. Point **b** ($U = 0.7405, M(U) = 15.01$ and $f = 70.59\ kHz$), in turn, corresponds to CCM when a current reference of 1.05 A is employed. Point **c** ($U = 0.856, M(U) = 48.3$ and $f = 88.23\ kHz$) represents the boundary between DCL2 and CCM for a load of $10k\Omega$. The corresponding inductor current waveforms are shown in figure 13.

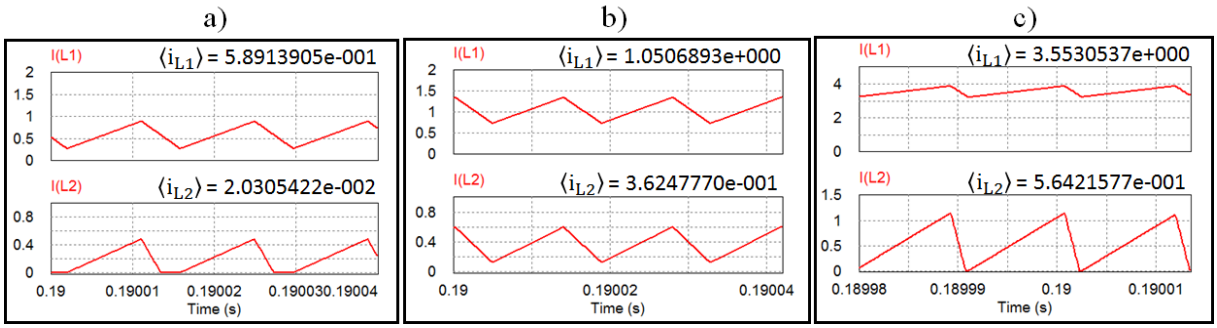

Fig.13. PSIM simulated waveforms of inductor currents for the operational points (a, b and c) in figure 12.

VI. EXPERIMENTAL RESULTS

A 80 W laboratory prototype of the quadratic boost converter and a computer- based test set-up have been built in order to validate the theoretical predictions and the simulation results. Several measurements verify the predicted waveforms and converter gains.

A. Experimental set-up and converter prototype

The power stage shown in figure 14 has been made with inductors $L_1 = 220\mu H$ and $L_2 = 820\mu H$ from Bourns Inc., two 1300 V thin film capacitors $C_1 = C_2 = 11\mu F$ from EPCOS, a 1200 V SiC MOSFET SCT2160KE from ROHM Semiconductor, and three 1200 V Schottky diodes C2D05120A from CEE. The converter has been controlled using both PWM and hysteresis modulation, and so two control circuits have been built. The PWM- based control has been developed using the PWM module of dsPIC30F4011 whose duty cycle can be modified through an A/D channel. The hysteresis comparator was implemented with basic discrete electronics.

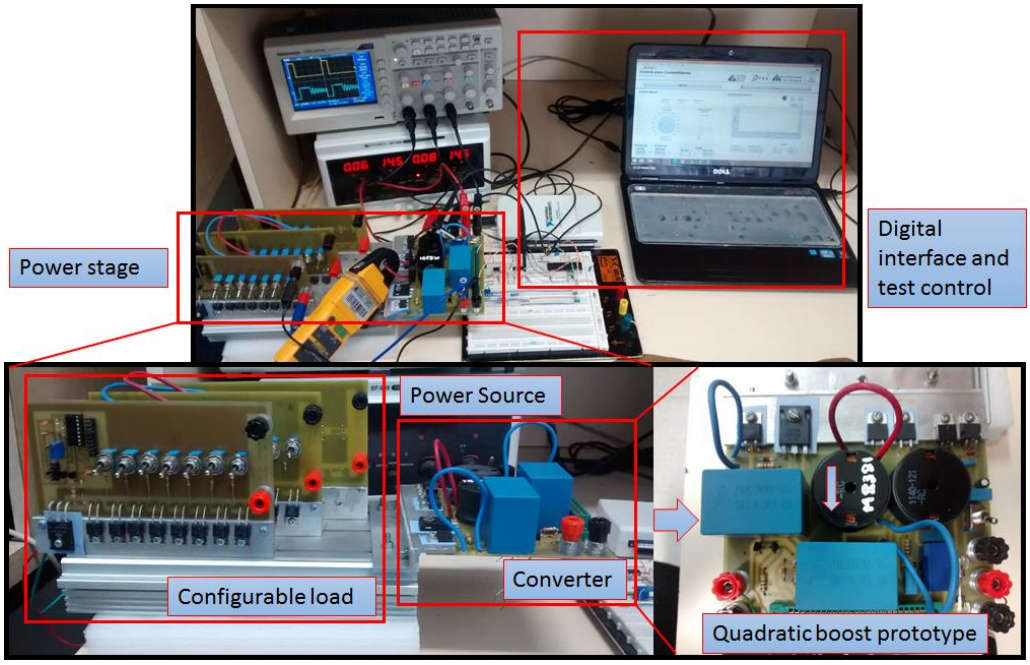

Fig.14. Converter prototype and experimental set-up

The measurement set-up shown in figure 14 is composed of an Oscilloscope TDS 2024C from Tektronix, a multimeter A830L from SMT, a power source EF-055 from Erasmus and a current probe I30s from Fluke. A computer- based test interface has been made using the acquisition card NI-USB-6210 from National Instruments and a LabVIEW application. The computer program defines a voltage to adjust the duty cycle of the PWM modulator and takes measurement samples of input and output voltages of the converter.

B. Inductor conduction modes and waveforms

Different operational points have been evaluated in order to obtain the four possible inductor conduction modes (CCM, DCL1, DCL2 and DCL12). Both inductor currents and voltages are depicted in figures 15, 16, 17 and 18 respectively. The gain of the converter at each point has been also verified.

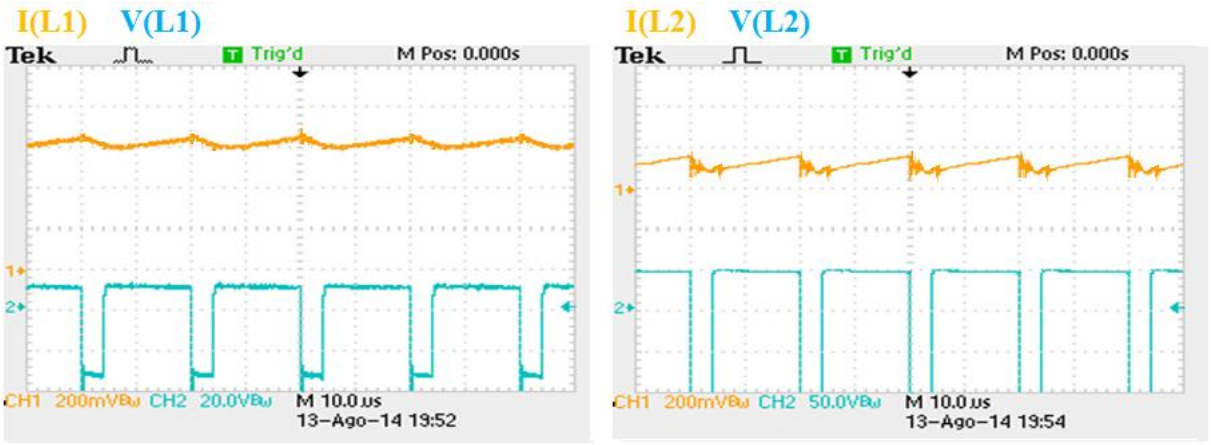

Fig.15. Current and voltage experimental waveforms for CCM.

(Parameters: $L_1 = 120\ \mu H, L_2 = 820\ \mu H, C_1 = C_2 = 10\ \mu F, R = 1.5\ k\Omega, V_i = 15\ V$ $f_s = 50\ kHz, D = 0.81$)

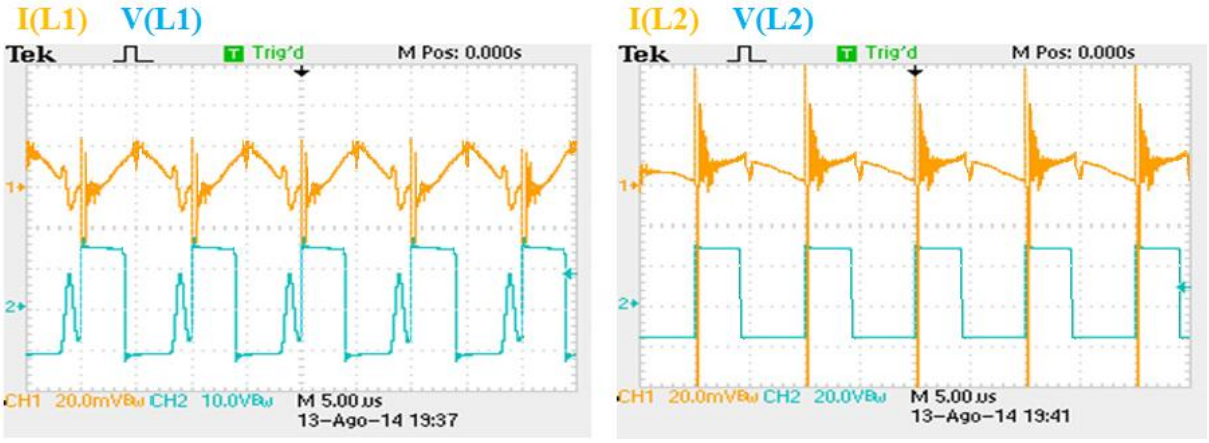

Fig.16. Experimental waveforms of inductor currents and voltages for DCM1.

(Parameters: $L_1 = 120\ \mu H, L_2 = 820\ \mu H, C_1 = C_2 = 10\ \mu F, R = 1\ k\Omega, V_i = 15\ V$ $f_s = 100\ kHz, D = 0.4$)

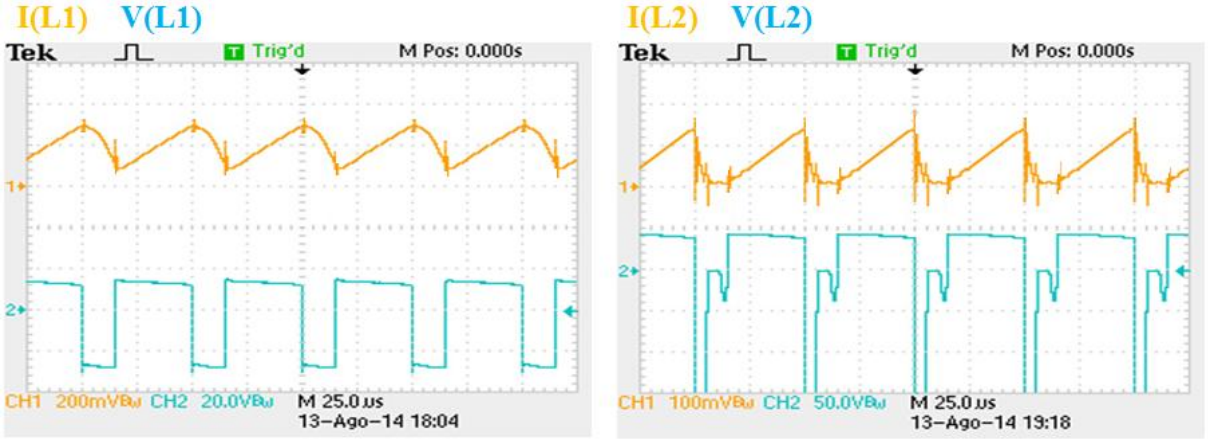

Fig. 17 Experimental waveforms of inductor currents and voltages for DCM2.

(Parameters: $L_1 = 120\ \mu H, L_2 = 820\ \mu H, C_1 = C_2 = 10\ \mu F, R = 5\ k\Omega, V_i = 15\ V$ $f_s = 20\ kHz, D = 0.7$)

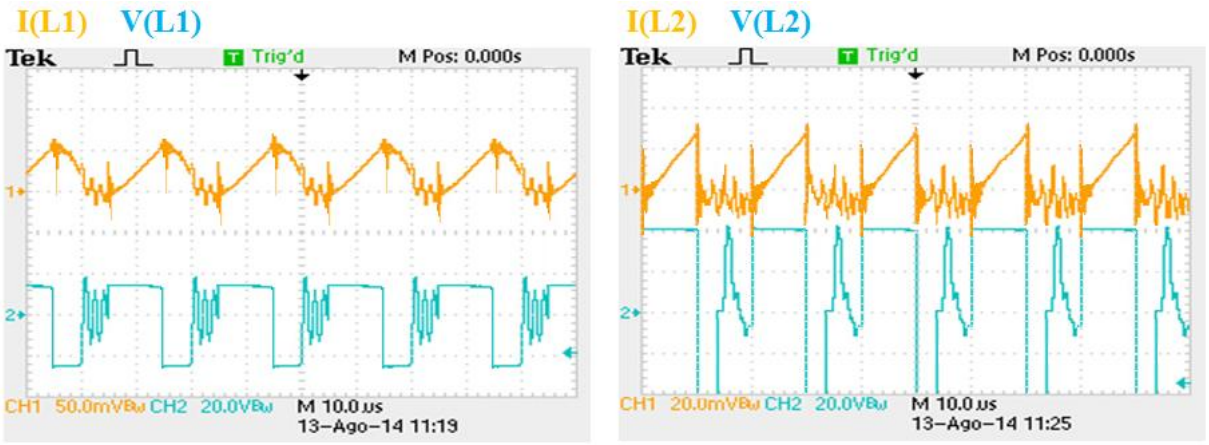

Fig.18.Experimental waveforms of inductor currents and voltages for DCM12.
($L_1 = 120\ \mu H, L_2 = 820\ \mu H, C_1 = C_2 = 10\ \mu F, R = 10\ k\Omega, V_i = 15\ V\ f_s = 50\ kHz, D = 0.5$)

C. Converter gain for constant switching frequency

Figure 19 shows the experimental converter gain curves when a PWM modulator is employed and a great number of samples are produced by means of the computerized variation of the duty cycle. The curves correspond to operation with constant resistive loads of $1k\Omega, 5k\Omega$ or $10k\Omega$ and show a distribution of the different conduction modes in each of them.

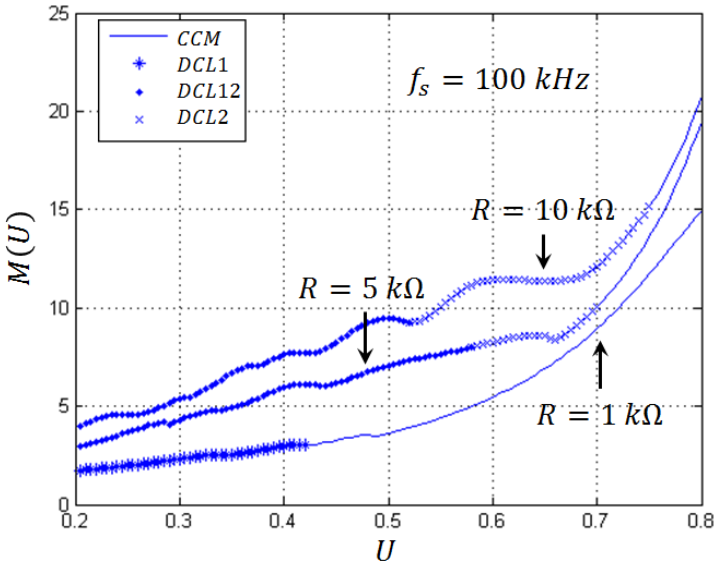

Fig.19. Measured converter gain vs. duty cycle with constant switching frequency operation

In comparison with the simulated results of figure 10, the static behavior keeps the same shape but the gain value is slightly affected by the voltage drops and power losses of the prototype. Hence, the theoretical and simulated results are in good agreement with the experimental results.

D. Converter gain for variable switching frequency

Figure 20 shows two experimental curves of the converter gain when a hysteresis modulator is employed. The curves correspond to operation with constant resistive loads of $1k\Omega$ or $6.6k\Omega$. A hysteresis band of ± 0.15 A has been used.

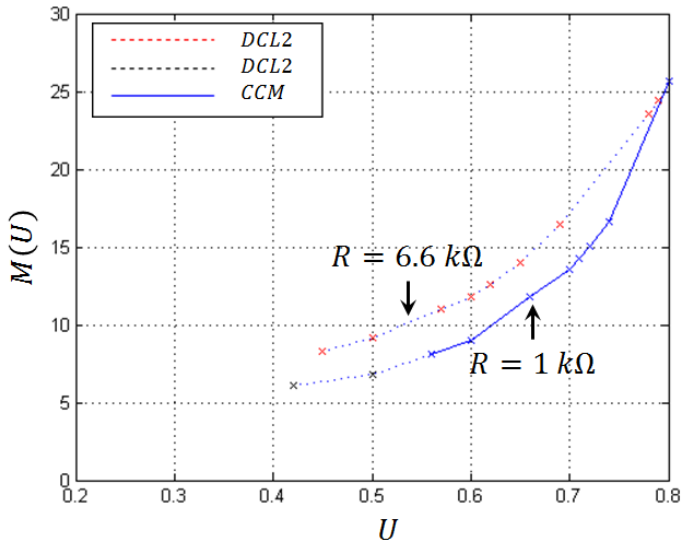

Fig.20. Measured converter gain vs. duty cycle with variable switching frequency operation

The gain of the converter with the hysteresis comparator shows a similar behavior to the simulation results shown in 12. Note also that the gain curve is very similar to that of PWM. However, the difference can be attributed to the effect of switching frequency diminution when the power load increases in the hysteresis case, which reduces the commutation losses allowing a higher gain especially for higher duty cycles. Excessively low duty cycles have been avoided to ensure proper operation of the hysteresis comparator.

E. Converter efficiency

In order to assess the efficiency of the quadratic boost converter prototype covering sufficient operational conditions to have a broad scope of comparison among conduction modes, several data have been obtained from experiments. The output voltage has been fixed at 400 V by means of a regulation loop in order to have a real operational condition such as the DC bus voltage in a grid-connected two- stage photovoltaic inverter. A test has been applied by changing the input voltage, the power load and the frequency in a coherent operational range. The results have been arranged in Table II for output power values of 16, 32, 48, 64 and 80 W. Although only Tables for 32 and 48 W are finally presented for the sake of brevity, this illustration is sufficient to reveal the most significant results relating the conduction mode and the efficiency of the converter.

TABLE II
Measurements of the converter variables for an output power of 32 W

$V_{C2}\ (V)$	$Freq$ (KHz)	$V_i\ (V)$	D	$V_{C1}(V)$	$I_{L1}(A)$	$I_{L2}\ (A)$	$\boldsymbol{\eta}$	*Mode*	$Pout\ (W)$
400	20	15	75.63	50.51	3.09	0.96	**0.6904**	DCL2	32
		20	68.64	57.21	2.16	0.84	**0.7407**	DCL2	
		25	56.29	69.07	1.68	0.72	**0.7619**	DCL12	
		30	45.71	82.51	1.38	0.6	**0.7729**	DCL12	
	40	15	81.18	64.68	2.98	0.72	**0.7159**	CCM	
		20	74.33	69.55	2.06	0.68	**0.7767**	DCL2	
		25	68.83	74.5	1.62	0.64	**0.7901**	DCL2	
		30	62.19	84.58	1.34	0.56	**0.7960**	DCL2	
	60	15	83	71	2.88	0.64	**0.7407**	CCM	
		20	78.26	82.56	1.99	0.56	**0.8040**	CCM	
		25	73.19	87.19	1.56	0.52	**0.8205**	CCM	
		30	68.69	91.89	1.28	0.52	**0.8333**	CCM	
	80	15	83.27	70.71	2.88	0.64	**0.7407**	CCM	
		20	79.59	84.91	2	0.56	**0.8000**	CCM	
		25	76.22	95.98	1.57	0.48	**0.8153**	CCM	
		30	72.43	102.95	1.28	0.44	**0.8333**	CCM	
	100	15	83.81	69.86	2.94	0.64	**0.7256**	CCM	
		20	79.93	84.35	2.05	0.56	**0.7805**	CCM	
		25	76.87	95.68	1.6	0.48	**0.8000**	CCM	
		30	74.34	105.55	1.32	0.44	**0.8080**	CCM	

TABLE III
Measurements of the converter variables for an output power of 48 W

$V_{C2}\ (V)$	$Freq$ (KHz)	$V_i\ (V)$	D	$V_{C1}(V)$	$I_{L1}(A)$	$I_{L2}\ (A)$	$\boldsymbol{\eta}$	*Mode*	$Pout\ (W)$
400	20	15	80.12	55.17	5.05	0.88	**0.6337**	DCL2	48
		20	72.48	62.8	3.22	0.84	**0.7453**	DCL2	
		25	67.19	69.35	2.48	0.76	**0.7742**	DCL2	
		30	56.37	81.7	2.04	0.62	**0.7843**	DCL2	
	40	15	83.76	68.34	4.68	0.64	**0.6838**	CCM	
		20	78.13	78.5	3.07	0.56	**0.7818**	DCL2	
		25	72.95	83.35	2.38	0.56	**0.8067**	DCL2	
		30	68.36	87.96	1.95	0.56	**0.8205**	DCL2	
	60	15	83.57	69.69	4.43	0.6	**0.7223**	CCM	
		20	79.79	84.33	3	0.48	**0.8000**	CCM	
		25	76.53	96.15	2.3	0.44	**0.8348**	DCL2	
		30	72.76	102.63	1.88	0.44	**0.8511**	DCL2	
	80	15	83.57	69.99	4.32	0.6	**0.7407**	CCM	
		20	79.79	85.43	2.93	0.48	**0.8191**	CCM	
		25	76.76	97.06	2.24	0.44	**0.8571**	CCM	
		30	74.19	107.12	1.86	0.4	**0.8602**	DCL2	
	100	15	83.82	69.76	4.46	0.64	**0.7175**	CCM	
		20	79.79	85.71	2.89	0.48	**0.8304**	CCM	
		25	76.76	97.27	2.22	0.44	**0.8649**	CCM	
		30	74.33	107.64	1.84	0.4	**0.8695**	CCM	

It can be shown in Tables II and III that some rows have been highlighted. These rows correspond to operational points with efficiencies higher than 80%, which are related with CCM and DCL2. It is worth to note that maximum efficiencies around 86% have been obtained in both CCM and DCL2 modes.

Mode DCL12 is only observed for low switching frequencies, input voltages between 25 and 30 V and lower power loads. Besides, considering a high DC gain application, DCL12 is almost unobservable. Mode DCL2 is reachable by both PWM and hysteresis modulation, and therefore operating in modes CCM and DCL2 is desirable. Particular interest offers the boundary mode between CCM and DCL2 because offers the advantages of both modes and avoids the drawbacks of the discontinuous conduction mode when the non-conduction time-interval of the inductor current is accentuated.

VII. CONCLUSIONS

In this work, the conduction modes of the quadratic boost converter have been disclosed and analyzed in steady-state when the converter operates using either a PWM or a hysteresis comparator. Besides the conventional CCM, four inductor current discontinuous conduction modes have been found and explored, namely, DCL1, DCL2, DCL12 and DCL21. In the context of high -DC gain applications, only DCL2 can be competitive in comparison with CCM because it can be attained with a normal set of parameters in both PWM and hysteresis cases exhibiting similar levels of efficiency. Particular interest offers operating in the boundary between CCM and DCL2 in order to exploit the advantages of both CCM and DCM. Regarding prospective work, the study of the dynamic behavior of the quadratic boost converter operating in DCL2 with a hysteresis modulator is in progress. A reduction of two in the system order would be expected if the converter were analyzed under the optics of sliding-mode control theory. Therefore, a second -order zero-dynamics would be apparently easier to handle than a third order dynamics of CCM for the design of a robust controller regulating the output voltage [51].

REFERENCES

[1] D. Maksimovic, S. Cuk, "A unified analysis of PWM converters in discontinuous modes," IEEE Trans. Power Electron., vol. 6, no. 3, pp. 476-490, Jul. 1991.

[2] V. Vorperian, "Simplified analysis of PWM converters using model of PWM switch. II. Discontinuous conduction mode," IEEE Trans. Aerospace and Electron. Systems, vol. 26, no. 3, pp. 497-505, May. 1990.

[3] N. Femia, V. Tucci, "On the modeling of PWM converters for large signal analysis in discontinuous conduction mode," IEEE Trans. Power Electron., vol. 9, no. 5, pp. 487-496, Sep. 1994.

[4] F. Guinjoan, J. Calvente, A.Poveda, L.Martinez, "Large-signal modeling and simulation of switching DC-DC converters," IEEE Trans. Power Electron., vol. 12, no. 3, pp. 485-494, May1997.

[5] S.-S. Hong, "Unified model of PWM switch including inductor in DCM," Electronics Letters, vol. 35, no. 1, pp. 10-11, Jan. 1999.

[6] J.-Y. Lee, H.-J. Chae, "6.6-kW Onboard Charger Design Using DCM PFC Converter With Harmonic Modulation Technique and Two-Stage DC/DC Converter," IEEE Trans. Ind. Electron., vol. 61, no. 3, pp. 1243-1252, Mar. 2014.

[7] C.W. Clark, F. Musavi, W. Eberle, "Digital DCM Detection and Mixed Conduction Mode Control for Boost PFC Converters," IEEE Trans. Power Electron., vol. 29, no. 1, pp. 347-355, Jan. 2014.

[8] X. Zhang, J.W. Spencer, "Analysis of Boost PFC Converters Operating in the Discontinuous Conduction Mode," IEEE Trans. Power Electron., vol. 26, no. 12, pp. 3621-3628, Dec. 2011.

[9] K. De Gusseme; D.M Van de Sype, A.P.M. Van den Bossche, J.A. Melkebeek, "Input-Current Distortion of CCM Boost PFC Converters Operated in DCM," IEEE Trans. Ind. Electron., vol. 54, no. 2, pp. 858-865, Apr. 2007.

[10] M.A. Chaudhari, H.M. Suryawanshi, "Analysis and design of three-phase rectifier operating in discontinuous conduction mode using high-frequency current injection technique," IET Power Electron., vol. 1, no. 4, pp. 419-432, Dec. 2008.

[11] Z. Zhang, M. Chen; W. Chen, C. Jiang, Z. Qian, "Analysis and Implementation of Phase Synchronization Control Strategies for BCM Interleaved Flyback Microinverters," IEEE Trans. Power Electron., vol. 29, no. 11, pp. 5921-5932, Nov. 2014.

[12] S. Zengin, F. Deveci, M. Boztepe, "Decoupling Capacitor Selection in DCM Flyback PV Microinverters Considering Harmonic Distortion," IEEE Trans. Power Electron., vol. 28, no. 2, pp. 816-825, Feb. 2013.

[13] T.-S. Hwang; S.-Y. Park, "Seamless Boost Converter Control Under the Critical Boundary Condition for a Fuel Cell Power Conditioning System," IEEE Trans. Power Electron., vol. 27, no. 8, pp. 3616-3626, Aug. 2012.

[14] Y.-C. Chuang; Y.-L. Ke; H.-S. Chuang; S.-Y. Chang, "Battery Float Charge Technique Using Parallel-Loaded Resonant Converter for Discontinuous Conduction Operation," IEEE Trans. Industry Applications, vol. 48, no. 3, pp. 1070-1078, May. 2012.

[15] A.M. Rahimi, A. Emadi, "Discontinuous-Conduction Mode DC/DC Converters Feeding Constant-Power Loads," IEEE Trans. Ind. Electron., vol. 57, no. 4, pp. 1318-1329, Apr. 2010.

[16] A. Khaligh, A. Emadi, "Mixed DCM/CCM pulse adjustment with constant power loads," IEEE Trans. Aerospace and Electronic Systems, vol. 44, no. 2, pp. 766-782, Apr. 2008.

[17] M. Zhu; F.L. Luo; Y. He, "Remaining Inductor Current Phenomena of Complex DC–DC Converters in Discontinuous Conduction Mode: General Concepts and Case Study," IEEE Trans. Power Electron., vol. 23, no. 2, pp.1014-1019, Mar. 2008.

[18] M. Ferdowsi, A. Emadi, "Estimative current mode control technique for DC-DC converters operating in discontinuous conduction mode," IEEE Power Electron. Letters, vol. 2, no. 1, pp. 20-23, Mar. 2004.

[19] C. Batlle, E. Fossas, I. Merillas, A. Miralles, "Generalized Discontinuous Conduction Modes in the Complementarity Formalism," IEEE Trans. Circuits and Systems II: Express Briefs, vol. 52, no. 8, pp. 447-451, Aug. 2005.

[20] J. Sun, D.M. Mitchell, M.F. Greuel, P.T. Krein, R.M. Bass, "Averaged modeling of PWM converters operating in discontinuous conduction mode," IEEE Trans. Power Electron., vol. 16, no. 4, pp. 482-492, Jul. 2001.

[21] C.-C. Fang, "Unified Discrete-Time Modeling of Buck Converter in Discontinuous Mode," IEEE Trans. Power Electron., vol. 26, no. 8, pp. 2335-2342, Aug. 2011.

[22] A. Davoudi, J. Jatskevich, T. De Rybel, "Numerical state-space average-value modeling of PWM DC-DC converters operating in DCM and CCM," IEEE Trans. Power Electron., vol. 21, no. 4, pp. 1003-1012, Jul. 2006.

[23] J.-W. Shin, B.-H. Cho, "Digitally Implemented Average Current-Mode Control in Discontinuous Conduction Mode PFC Rectifier," IEEE Trans. Power Electron., vol. 27, no. 7, pp. 3363-3373, Jul. 2012.

[24] S.F. Lim, A.M. Khambadkone, "A Simple Digital DCM Control Scheme for Boost PFC Operating in Both CCM and DCM," IEEE Trans. Industry Applications, vol. 47, no. 4, pp. 1802-1812, Jul. 2011.

[25] Y. Qiu, X. Chen, H. Liu, "Digital Average Current-Mode Control Using Current Estimation and Capacitor Charge Balance Principle for DC–DC Converters Operating in DCM," IEEE Trans. Power Electron., vol. 25, no. 6, pp. 1537-1545, Jun. 2010.

[26] Z.Z. Ye, M.M. Jovanovic, "Implementation and performance evaluation of DSP-based control for constant-frequency discontinuous-conduction-mode boost PFC front end," IEEE Trans. Ind. Electron., vol. 52, no. 1, pp. 98-107, Feb. 2005.

[27] K. De Gusseme, D.M. Van de Sype, A.P.M. Van den Bossche, J.A. Melkebeek, "Digitally controlled boost power-factor-correction converters operating in both continuous and discontinuous conduction mode," IEEE Trans. Ind. Electron., vol. 52, no. 1, pp. 88-97, Feb. 2005.

[28] M. Salimi, J. Soltani, G.A. Markadeh, N.R. Abjadi, "Indirect output voltage regulation of DC-DC buck/boost converter operating in continuous and discontinuous conduction modes using adaptive backstepping approach," IET Power Electron., vol. 6, no. 4, pp. 732-741, Apr. 2013.

[29] A. Alawieh, R. Ortega, H. Pillai, A. Astolfi, E. Berthelot, "Voltage Regulation of a Boost Converter in Discontinuous Conduction Mode: A Simple Robust Adaptive Feedback Controller," IEEE Control Systems, vol. 33, no. 3, pp. 55-65, Jun. 2013.

[30] K.-S. Leung, H.S.-H. Chung, "A Comparative Study of Boundary Control With First- and Second-Order Switching Surfaces for Buck Converters Operating in DCM," IEEE Trans. Power Electron., vol. 22, no. 4, pp. 1196-1209, Jul. 2007.

[31] A. Reatti, M.K. Kazimierczuk, "Small-signal model of PWM converters for discontinuous conduction mode and its application for boost converter," IEEE Trans. Circuits and Systems I: Fundamental Theory and Applications, vol. 50, no. 1, pp. 65-73, Jan. 2003.

[32] S.C. Tan, Y.M. Lai, C.K. Tse, L. Martinez-Salamero, "Special family of PWM-based sliding-mode voltage controllers for basic DC-DC converters in discontinuous conduction mode," IEE Proc. Electric Power Applications, vol. 1, no. 1, pp. 64-74, Jan. 2007.

[33] E. Babaei, M.E. Seyed Mahmoodieh, "Analysis and investigation of energy transmission process in different operating modes of SEPIC converter," IET Power Electron., vol. 7, no. 4, pp. 819-828, Apr. 2014.

[34] A. Davoudi, J. Jatskevich, P.L. Chapman, A. Khaligh, "Averaged-Switch Modeling of Fourth-Order PWM DC–DC Converters Considering Conduction Losses in Discontinuous Mode," IEEE Trans. Power Electron., vol. 22, no. 6, pp. 2410-2415, Nov. 2007.

[35] M.J. Willers, M.G. Egan, S. Daly, J.M.D. Murphy, "Analysis and design of a practical discontinuous-conduction-mode BIFRED converter," IEEE Trans. Ind. Electron., vol. 46, no. 4, pp. 724-733, Aug 1999.

[36] S.-K. Chung, "Transient characteristics of high-voltage flyback transformer operating in discontinuous conduction mode," IEE Proc. Electric Power Applications, vol. 151, no. 5, pp. 628-634, Sep. 2004.

[37] D.-H. Kim, G.-Y. Choe, B.-K. Lee, "DCM Analysis and Inductance Design Method of Interleaved Boost Converters," IEEE Trans. Power Electron., vol. 28, no. 10, pp. 4700-4711, Oct. 2013.

[38] H. Choi, L. Balogh, "A Cross-Coupled Master–Slave Interleaving Method for Boundary Conduction Mode (BCM) PFC Converters," IEEE Trans. Power Electron., vol. 27, no. 10, pp. 4202-4211, Oct. 2012.

[39] L. Huber, B.T. Irving, M.M. Jovanovic, "Open-Loop Control Methods for Interleaved DCM/CCM Boundary Boost PFC Converters," IEEE Trans. Power Electron., vol. 23, no. 4, pp. 1649-1657, Jul. 2008.

[40] S. Cûk, "Discontinuous Inductor Current Mode in the Optimum Topology Switching Converter," in Proc. Power Electronics Specialist Conference (PESC), 1978, pp. 105-123.

[41] C.-Y. Chiang, C.-L. Chen, "Zero-Voltage-Switching Control for a PWM Buck Converter under DCM/CCM Boundary," IEEE Trans. Power Electron., vol. 24, no. 9, pp. 2120-2126, Sep. 2009.

[42] J. Sebastian, J.A. Cobos, J.M. Lopera, J. Uceda, "The determination of the boundaries between continuous and discontinuous conduction modes in PWM DC-to-DC converters used as power factor preregulators," IEEE Trans. Power Electron., vol. 10, no. 5, pp. 574-582, Sep. 1995.

[43] A. Leon-Masich, H.Valderrama-Blavi, J.M.Bosque-Moncusi, J.Maixe-Altes, L.Martinez-Salamero, "Sliding-mode control –based boost converter for high-voltage low- power applications," IEEE Trans. Industrial Electron., vol. 62, no. 1, pp. 229-237, Jan. 2015.

[44] J.A. Abu Qahouq,"Control Scheme for Sensorless Operation and Detection of CCM and DCM Operation Modes in Synchronous Switching Power Converters," IEEE Trans. Power Electron., vol. 25, no. 10, pp. 2489-2495, Oct. 2010.

[45] R.W. Erickson, D. Maksimovic. Fundamentals of power electronics. Kluwer Academic Publishings, 1999.

[46] M.G. Ortiz-Lopez, J. Leyva-Ramos, E.E. Carbajal-Gutierrez , J.A. Morales-Saldaña, "Modelling and analysis of switch-mode cascade converters with a single active switch," IET Power Electron., vol. 1, no. 4, pp. 478-487, Dec. 2008.

[47] J. Leyva-Ramos, M.G. Ortiz-Lopez, L.H. Diaz-Saldierna ,J.A. Morales-Saldaña, "Switching regulator using a quadratic boost converter for wide DC conversion ratios," IET Power Electron., vol. 2, no. 5, pp. 605-613, May 2009.

[48] G. AlLee, W. Tschudi, "Edison Redux: 380 Vdc Brings Reliability and Efficiency to Sustainable Data Centers," IEEE Power and Energy Magazine, vol. 10, no. 6, pp. 50-59, Nov. 2012.

[49] B.T. Patterson, "DC, Come Home: DC Microgrids and the Birth of the "Enernet"", IEEE Power and Energy Magazine, vol. 10, no. 6, pp. 60-69, Nov. 2012.

[50] O. Lopez-Santos, L. Martinez-Salamero, G. Garcia, H. Valderrama-Blavi and D.O. Mercuri, "Efficiency analysis of a sliding-mode controlled quadratic boost converter," IET Power Electron., vol. 6, no. 2, pp. 364-373, Feb. 2013.

[51] O. Lopez-Santos, L. Martinez-Salamero, G. Garcia, H. Valderrama-Blavi, H.; T. Sierra-Polanco, "Robust Sliding-Mode Control Design for a Voltage Regulated Quadratic Boost Converter," IEEE Trans. Power Electron., vol. 30, no. 4, pp. 2313-2327, Apr. 2015.